Thermal Modeling of a Surface-micromachined Linear Thermomechanical Actuator

C. D. Lott, T. W. McLain, J. N. Harb, L. L. Howell
Brigham Young University, Provo, UT, USA

ABSTRACT

The thermal behavior of a thermomechanical in-plane microactuator is modeled using a finite-difference approach. Steady-state temperature profiles from the model are presented for a microactuator operating in air and a vacuum. The model is validated by comparing the actuator displacements predicted by the model with those obtained experimentally. Initial results demonstrate significant improvements in the steady-state efficiency of the microactuator when it is operated in a vacuum.

Keywords: microactuator, thermomechanical actuator

1 INTRODUCTION

The development of microactuators and an understanding of their behavior will play a key role in the realization of autonomous microelectromechanical systems (MEMS). Thermomechanical microactuators have shown promise for MEMS applications due to their relatively large force and displacement capabilities. In addition, they can be fabricated using conventional integrated circuit (IC) technology and driven by CMOS compatible voltages and currents.

This paper treats the thermal modeling of a particular type of thermomechanical actuator called the thermomechanical in-plane microactuator (TIM) [1]. As shown in Figure 1, the basic TIM design consists of a moveable shuttle connected to electrical contact pads on the substrate by slender thermal expansion legs. As a voltage difference is applied across the contact pads, current flows through the legs and the shuttle. The high current density in the legs causes ohmic heating and thermal expansion. The legs are connected to the shuttle at a slight angle so that their expansion causes linear motion of the shuttle.

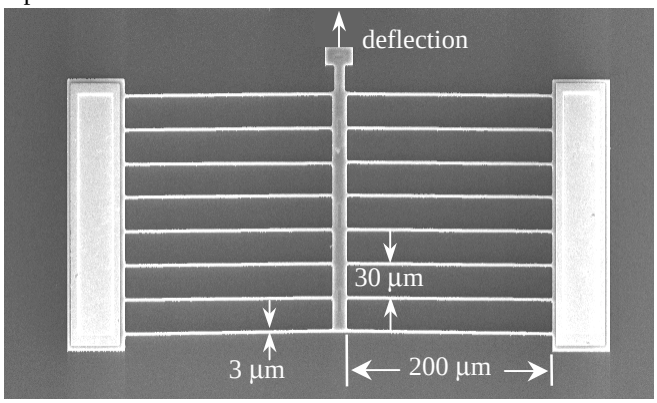

Figure 1. Thermomechanical in-plane microactuator (TIM)

One potential weakness of thermally actuated devices, from an energy perspective, is inefficiency. The need exists, therefore, to understand how to best raise the temperature in the legs to get a desired deflection using minimal energy. In this paper, the thermal response of a TIM device is examined by creating a finite-difference model with temperature-dependent parameters. The model, which has been validated using measurements from several tests, allows temperatures throughout the device to be simulated as a function of time. The effect on efficiency, resulting from design changes to the TIM, can be investigated with the model. Insights gained from this model have resulted in significant improvements in operational efficiency of the microactuator. All of the TIMs simulated and tested were fabricated using the Multi-User MEMS Processes (MUMPs) from Cronos [2].

2 MODEL

In modeling the heat transfer in the TIM device, a one-dimensional treatment for heat conduction in the legs is used since the length dimension is much larger than any dimension of the cross-section. The portion of the TIM device modeled here consists of a shuttle suspended above the substrate by two legs as shown in Figure 2. The heat transfer in a multiple-leg-pair device, such as that shown in Figure 1, can be modeled using a single-leg-pair model under the assumption that each pair of legs is thermally independent.

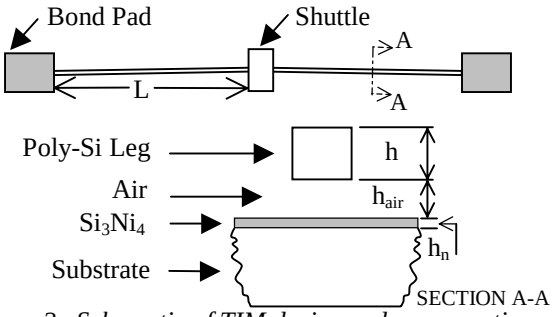

Figure 2. Schematic of TIM device and cross-section

In order to set up the finite-difference model, the device in Figure 2 was divided into discrete volume elements. By applying an energy balance to a control volume around each element, a state equation is formulated for each. When solved, the set of equations for all elements produces the nodal temperatures throughout the body. Based on an energy balance, the following state equation is obtained for the i^{th} element

$$q_i + q_{cond} + q_{rad} + q_{cond,i-1} + q_{cond,i+1} = q_{st}\,, \qquad (1)$$

where q_i is the rate of energy generated in element i by ohmic heating, q_{cond} models conduction to the substrate, and q_{rad} models radiation to the surroundings. The conduction to element i from adjoining elements is modeled by the $q_{cond,i-1}$ and $q_{cond,i+1}$ terms. Energy storage within the element is modeled by q_{st}. Because the contribution of free convection has been found to be small, it is not included in the energy balance [3-5].

Each of these energy terms can be determined from straightforward physical relationships. Ohmic heating can be calculated from the input current and material resistivity $\rho_r(T)$ as

$$q_i = J^2 \rho_r(T) \Delta V_i \tag{2}$$

where J is the current density input to the system and ΔV_i is the element volume. Conduction to the substrate is modeled by the expression

$$q_{cond} = \frac{SA_u}{G_u}\left[T_{sub} - T_i(k)\right] \tag{3}$$

where T_{sub} is the temperature of the substrate (assumed constant) and $T_i(k)$ is the temperature of the i^{th} node at the k^{th} time increment. A_u represents the area of the element's surface that faces the substrate. S is a shape factor that accounts for conduction from the vertical faces of the element to the substrate. For a beam shaped microbridge, S can be expressed as [4]

$$S = \frac{h}{w} \cdot \left(\frac{2 \cdot h_{air}}{h} + 1 \right) + 1 \tag{4}$$

where h is the height of the element, w is the width, and h_{air} is the height of the air gap between the leg and the substrate. From Figure 2b, it is evident that the heat path to the substrate is through the air and an electrically insulated layer of silicon nitride. These layers act as two thermal paths in series, allowing G_u to be defined as

$$G_u = \frac{h_{air}}{k_{air}} + \frac{h_n}{k_n} \tag{5}$$

where h_n is the height of the Si_3Ni_4 layer.

Radiation to the surroundings is negligible at low temperatures. However, for the high temperatures and vacuum environments considered here, it can have an effect. The energy radiated to the surroundings can be expressed as

$$q_{rad} = \varepsilon \sigma A_s [T_{sur}^4 - T_i^4(k)] \tag{6}$$

where A_s is the area of the exposed surface of the element.

Conduction of heat between element $i-1$ and element i is modeled by the expression

$$q_{cond,i-1} = \frac{k_p A_x}{\Delta x}\left[T_{i-1}(k) - T_i(k)\right]. \tag{7}$$

A_x is the cross-sectional area of the element, Δx is the length of the element in the direction of heat transfer and k_p is the thermal conductivity of polysilicon. Finally, storage of thermal energy within each element is calculated as

$$q_{st} = \frac{\rho c \Delta V_i}{\Delta t}\left[T_i(k+1) - T_i(k)\right] \tag{8}$$

where ρ and c are the density and specific heat of polysilicon and Δt is the time increment.

By substituting Equations 2 through 8 into Equation 1, an expression for the nodal temperatures at time $k+1$ in terms of nodal temperatures at time k , the current input, and the boundary conditions (T_{sur} and T_{sub}) can be formed. By solving the system of difference equations from all of the elements over a series of time increments, a profile of temperatures throughout the device versus time can be produced.

Table 2 lists parameter values used in the model. Thermal conductivity of polysilicon was treated in two different ways in the model: as a constant and as a function of temperature. When modeled as being constant, k_p was taken to be 30 W/m C [5,7]. As a function of temperature, k_p was calculated using the expression [8]

$$k_p(T) = \left[\left(-2.2\times10^{-11}\right)T^3 + \left(9.0\times10^{-8}\right)T^2 + \left(-1.0\times10^{-5}\right)T + 0.014\right]^{-1}. \tag{9}$$

Table 2. Model parameters

Parameter	Value	Ref.
Emissivity of polySi	$\varepsilon = 0.6$	3
Therm cond of Si_3Ni_4	$k_n = 2.25\ W/m \cdot C$	3
Therm cond. of air	$k_{air} = 0.026\ W/m \cdot C$	6
Specific heat	$c = 700\ J/kg \cdot C$	4
Density	$\rho = 2330\ kg/m^3$	5
Stefan-Boltzmann	$\sigma = 5.67 \times 10^{-8}\ W/m^2 \cdot K^4$	6
Resistivity	$\rho_r(T) = \rho_0[1 + \beta(T - T_s)]$	5
	$\rho_0 = 2.4\times10^{-3}\ \Omega \cdot cm$	9
	$\beta = 1.25 \times 10^{-3}\ \ C^{-1}$	7

Simulations were based on a TIM design having a leg length of 250 μm and shuttle dimensions of 50 μm by 30 μm. The boundary conditions applied to the TIM model assume that the temperature of the anchored bond pads, T_{sub}, and the surrounding temperature, T_{sur}, remain constant at 20 C. Each leg was divided into 25 elements of equal length. Based on the size of the elements chosen, a constant time step of 1 μs was used [6].

For validation purposes, simulation results from the finite difference model are compared to those obtained from an analytical expression modeling the TIM under steady-state conditions [3]. At steady-state, a balance between all energy rates on a differential element requires that resistive heating power generated within the element be equal to heat conducted out. Ignoring radiation and free convection, the following expression results

$$\frac{\partial}{\partial x}\left(k_p \frac{\partial T}{\partial x}\right) + \dot{q} - S\frac{(T - T_s)}{G_u \cdot h} = 0\,. \tag{10}$$

Here, $\dot{q}$ is the rate of energy generation per unit volume due to ohmic heating. This equation has a closed-form solution that describes the temperature versus position along the leg.

3 MODELING RESULTS

Figure 3 shows the steady-state temperature profiles obtained for a two-leg TIM in air with a constant 5.6 mA input. From the profiles, it is clear that the analytical solution from Equation (10) and the constant-k_p finite-difference solution are in good agreement as expected. Since the constant-k_p finite-difference model includes radiation to the surroundings, its temperature profile is slightly lower (1.7 percent at the peak temperatures). Because heat is conducted efficiently through the air from the shuttle to the substrate, the shuttle temperature is significantly lower than that of the legs.

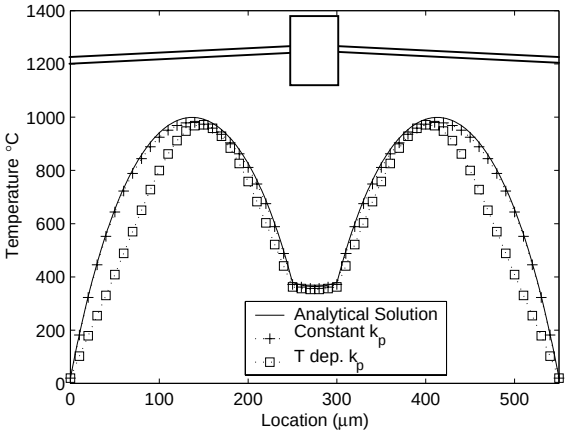

Figure 3. Steady-state profile in air at 5.6 mA

Figure 3 also shows that a slightly different temperature profile is obtained when the thermal conductivity for polysilicon is considered to be temperature dependent. At low temperatures, the temperature-dependent k_p value is higher than the constant value used. This results in lower steady-state temperatures near the bond pad when the temperature-dependent expression is used. At high temperatures, the value of k_p is nearly the same. This causes the portions of the leg near the shuttle and their nodal temperatures to be similar to those obtained from the constant-k_p model.

In a vacuum, the resulting temperature profiles are noticeably different as Figure 4 shows. Because no heat is conducted to the substrate in a vacuum (which is the primary heat transfer method in air), the shuttle temperature rises and eventually becomes the highest temperature in the actuator.

To simulate the vacuum environment the q_{cond} term in Equation (1), which represents heat conduction down to the substrate, was eliminated from the model. This has the effect of insulating the TIM, leaving conduction through the legs to the bond pads and radiation of heat to the

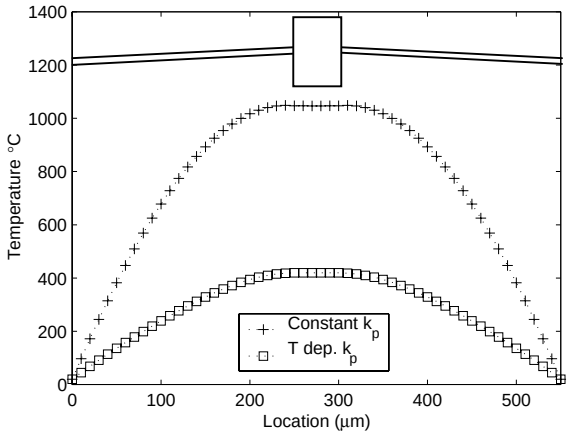

Figure 4. Steady-state profile in vacuum at 1.6 mA

surroundings as the only paths for heat flow. With this insulating effect, the TIM in the vacuum reaches similar steady-state peak temperatures as attained in air with a much lower input current. Comparing the constant-k_p results from Figures 3 and 4 shows that in a vacuum, an input current of 1.6 mA causes a slightly higher peak temperature than 5.6 mA in air. Since actuator displacement increases with leg temperature, this indicates that TIM devices can be operated with much improved steady-state efficiency in a vacuum.

For the 1.6 mA vacuum results shown in Figure 4, the difference between the constant-k_p model and the temperature-dependent-k_p model is more pronounced than in air at 5.6 mA. For slightly higher currents, this difference in temperature profiles decreases significantly as the legs become hotter and the difference in the k_p values between the two models is much smaller. For example, at 1.8 mA, the peak temperatures between the two models differ only by 33 percent.

4 MODEL VALIDATION

Because of the difficulty in measuring temperatures directly from the TIM, indirect approaches were used to validate the model. The first approach involved using the nodal temperatures from the model as inputs to a commercial finite-element code (Ansys 5.5) to predict the steady-state shuttle deflection and then comparing this with the shuttle deflection measured experimentally under the same conditions.

Figures 5 and 6 show how experimental measurements of deflection match the Ansys results. In air, good correlation is found between the predicted results and the different material setups chosen. As Figure 5 shows, the best fit to the measured data was obtained by using a k_p that is dependent on temperature. Figure 6 shows deflection data for a vacuum. For small current inputs, the temperature-dependent k_p value gives the best results, but this changes significantly as the current is increased. For larger current inputs, the constant-k_p model provides a better correlation

with the experimental measurements. Because the experimentally observed displacements are sensitive to numerous other variables besides temperature (e.g., stiction), further testing needs to be done to resolve which model is most consistent with experimental results.

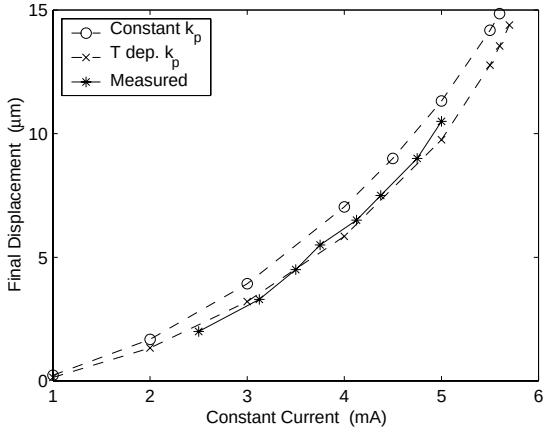

Figure 5. Shuttle displacement vs. current in air

A second validation approach involved photographing the TIM at specific current inputs and looking for two things: the onset and location of visible radiation or the beginning of a small glow, and the charring or destruction of the legs at the melting temperature. Figure 7 shows an example photograph for the TIM in air. The glowing of the legs shows that the position of high-temperature regions observed experimentally are consistent with those obtained from the model (see Figure 3).

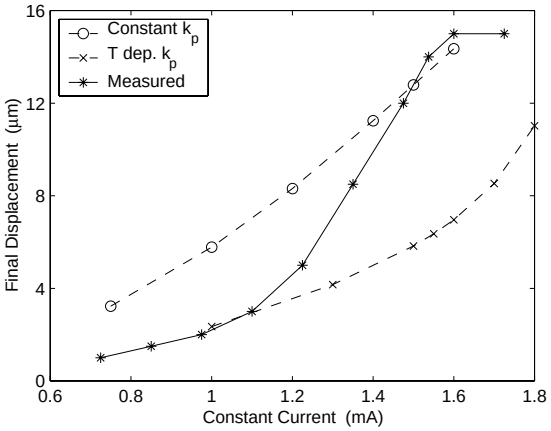

Figure 6. Shuttle displacement vs. current in vacuum

Photographs similar to Figure 7 have confirmed that less current is required to deflect the TIM in a vacuum than in air as the model predicts. Figure 8 shows the predicted steady-state power required to heat the TIM in air and a vacuum. In air, almost 50 mW per leg are needed to get the same rise in the average leg temperature that 6 mW will achieve within a vacuum. This result confirms that a significantly lower steady-state power is needed in a vacuum to obtain the same average temperature rise in the expansion legs.

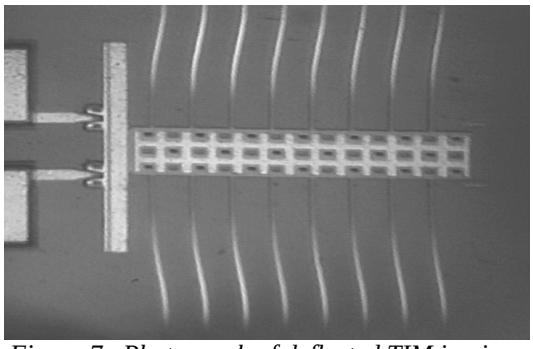

Figure 7. Photograph of deflected TIM in air

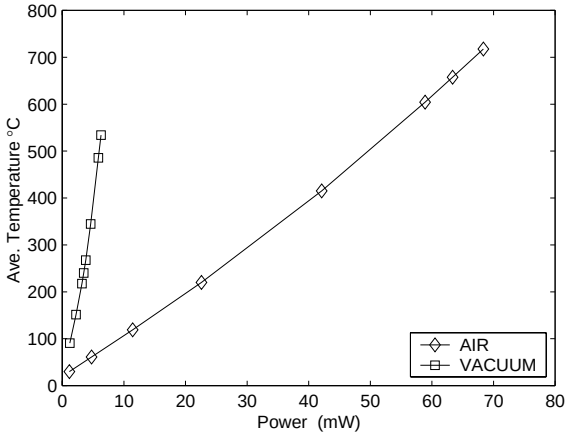

Figure 8. Steady-state leg temperature vs. power input.

5 CONCLUSIONS

A finite-difference thermal model for a TIM device has been developed. Indirect validations comparing experimentally measured shuttle displacements with those predicted by the thermal model (in conjunction with a commercial finite-element code) show good agreement in air. Results in a vacuum are less satisfactory but support the predicted trend. The model predicts that in a vacuum significantly lower steady-state input currents can be used to actuate a TIM device than in air. Experimental results have demonstrated this improvement as well.

REFERENCES

[1]. Cragun, R. and Howell, L., 1999 "Linear Thermomechanical Microactuators," ASME IMECE MEMS, pp. 181-188.

[2]. Mehregany, M. and Dewa, A.S., 1993, "Introduction to Microelectromechanical Systems and the Multi-user MEMS Process," MCNC and Case Western Reserve University.

[3]. Huang, Q. and Lee, N., 1999, "Analysis and design of polysilicon thermal flexure actuator," *J of Micromechanics and Microengineering*, Vol 9, pp. 64-70.

[4]. Lin, L. and Chiao, M. 1996, "Electrothermal responses of lineshape microstructures," Sensors and Actuators, Vol 55, pp. 35-41.

[5]. Mastrangelo, C.H., 1991, "Thermal applications of microbridges," Ph.D. Dissertation, U.C. Berkeley.

[6]. Holman, J.P., 1997, "Heat Transfer," 8th Ed., McGraw-Hill, p. 178.

[7]. Butler, J. and Bright, V., 1998, "Electrothermal and Fabrication Modeling of Polysilicon Thermal Actuators," DSC-Vol. 66, Micro Electro-Mechanical Systems (MEMS), pp. 571-576.

[8]. Manginell, R., 1997, "Polycrystalline-Silicon Microbridge Combustible Gas Sensor," Ph.D. Dissertation, Univ. of New Mexico.

[9]. http://www.memsrus.com/cronos/svcsdata.html